Title: Performance of real evapotranspiration products and water yield estimations in Uruguay

Gallego F.[a*], Camba Sans G.[b], Di Bella C.M.[b,e], Tiscornia G.[c], and Paruelo J.M.[a,b,d,e]

[a] Instituto de Ecología y Ciencias Ambientales, Facultad de Ciencias, Universidad de la República. Iguá 4225, Montevideo, Uruguay

[b] Departamento de Métodos Cuantitativos y Sistemas de Información. Facultad de Agronomía. Universidad de Buenos. Av. San Martín 4453, Buenos Aires, Argentina. carlos.m.dibella@gmail.com; camba@agro.uba.ar

[c] Instituto Nacional de Investigación Agropecuaria (INIA), Estación Experimental Las Brujas, Ruta 48 km 10, Canelones, Uruguay. gtiscornia@inia.org.uy

[d] Instituto Nacional de Investigación Agropecuaria (INIA), Estación Experimental La Estanzuela, Ruta 50 km 11, Colonia, Uruguay. jparuelo@inia.org.uy

[e] IFEVA – CONICET. Av. San Martín 4453, Buenos Aires, Argentina

*Corresponding author: fgallego@fcien.edu.uy; Iguá 4225, Montevideo, Uruguay. CP:11400. Phone: +598-25258621

Abstract

Real evapotranspiration (ETR) is a key variable in socio-ecological systems since it is related to the food supply, climate regulation, among others. Also, ETR strongly determines the water yield (WY) at the catchment level (water available for consumption or irrigation). In that sense, quantifying ETR and WY fluctuations linked to various human pressures is essential for comprehensive water planning. In the last decades, remote sensing ETR estimations have become increasingly performed worldwide for hydrological monitoring. In Uruguay, there are several attempts to quantify the ETR through different approaches. However, assessments related to the performance of the estimates of different sources/products, particularly from remote sensing, are still lacking. The main objectives of this article were: a) to evaluate the performance of different spatial explicit approaches to estimate real ETR and b) to estimate and analyse the variability in water yield derived from the different ETR sources/products for three climatically contrasting years. To achieve this, we used four remote sensing ETR products (PMLv2, MOD16A2, Jackson et al. 1977 and Di Bella et al. 2000), with different spatial and temporal resolutions (from 500 to 1000-m and 8 to 16-d), and two water balance models at two scales, national (INIA-GRAS) and micro-watershed level (Silveira et al. 2016). Our results suggest that MODIS and PMLv2 remote sensing products demonstrated better performances. Both products have high spatial (500-m) and temporal (8-d) resolution, captured seasonal differences between land-covers and showed positive and high correlations with the annual precipitation and productivity. The differences found between products have direct implications on the WY estimates, not only in the quantity but also in its spatial pattern. Future studies should explore MODIS and PML ETR estimations for understanding hydrological and ecological processes, global climate change research, agricultural drought detection and mitigation, and water resource management.

Keywords: remote sensing, land-cover, water balance, NDVI, precipitation.

1. Introduction

Real evapotranspiration (ETR) is a key variable in socio-ecological systems since it is related to the supply of many ecosystem services such as water availability for consumption or irrigation, food supply, climate regulation, among others (Rockström et al. 1999; Paruelo et al. 2016). ETR is defined as the sum of the plant canopy transpiration and the soil evaporation. Transpiration is the largest component of the terrestrial hydrologic cycle (Jasechko et al. 2013; Schlesinger and Jasechko, 2014) and is a critical factor in the water and carbon cycles (Chapin III et al. 2011). Climate (temperature and precipitation) and vegetation (i.e., plant functional types) are two of the main controls over the ETR (Chapin III et al. 2011). In the actual scenario of climate change (characterized by an increase in mean temperature and changes in the variability and seasonality of precipitation) and land-use changes (characterized by the replacement of natural ecosystems to anthropic ones), it becomes critical to estimate the ETR at different spatial and temporal scales to understand how ecosystems respond and feedback, and how the provision of key ecosystem services is affected.

ETR variations (in space and time) are associated with several factors, including vegetation types, soil water availability, cover and texture, climatic conditions (including extremes), and management strategies, among others. Regarding vegetation types, different land-covers differ in the total amount of water transpired. For example, Nosetto et al. (2005) found that the replacement of grasslands by Pinus and Eucalyptus plantations, in temperate subhumid areas of South America, generated a drastic change in evapotranspiration, where forest plantations consumed 80% more water than the native grasslands replaced. In terms of management strategies, ETR can vary, for example, under different grazing intensities (e.g. Bremer et al. 2001), degree of fertilization (e.g. Viets, 1962), botanical composition of the land-use (e.g. Bajgain et al. 2020) or associated with the use of irrigation systems (e.g. Bastiaanssen et al. 2000). Furthermore, ETR varies in different climatic conditions, such as dry and wet years. do Santos et al. (2020) reported, for the Caatinga biome of Brazil, a reduction of 25% in the mean annual ETR for dry years.

One of the main factors that determine the water yield (WY) at catchment level is the ETR. The WY is defined as the production of water from the catchments (Salemi et al. 2012). Since it may be readily accessed for human consumption, it is also known as "the blue water", in contrast to the “green water” which is consumed by plants (Falkenmark and Rockström, 2006). Because it supports wildlife, stream functioning, agricultural products, drinking water supply, and other ecosystem functions, it is obvious that the WY constitutes a critical socio-ecological variable. In such a way, quantifying WY fluctuations linked to various human pressures is essential for comprehensive water planning (Vörösmarty et al. 2000a, 2000b; Vörösmarty et al. 2015).

In general, different management strategies are increasingly used to minimize the intra- and inter-annual variability of the ETR. Among the most common management practices is the use of irrigation. Uruguay, and the region, have experienced several episodes of drought in the last 5 decades, with different intensities and extents (e.g. Lessel et al. 2016). Among the main consequences of drought are the economic ones. During a drought period, farmers in Uruguay have lost animals and sold cattle at a low price (Cruz et al. 2018), and crop yields have been affected (Lessel et al. 2016). Some current projections highlight an increase in the frequency and intensity of droughts (Dai, 2013; Cook et al. 2014). In Uruguay, this has led to the enactment of the Law Nº. 16.858 (Decreto Nº. 366/018 of November 2018), commonly known as the "Irrigation Law". This law aims to increase the country's agricultural production, giving greater stability to crops (mainly soybean, corn, and rice) and sown pastures beyond the rainfall regime. However, many decisions like irrigation strategies, or subsidies for water allocations are made with partial information of the magnitude of change in ETR, due to the spatial and temporal complexity of its estimation.

ETR can be measured using several in-situ techniques such as weighing lysimeters, Sap-flow systems, Eddy Covariance systems, Bowen stations, etc. or estimated by satellite remote sensing data or calculated from water and energy balances (Wilson et al. 2001; Ford et al. 2007; Kosugi and Katsuyama, 2007; Bhattarai and Wagle, 2021). In situ techniques can provide long-term point or local scale observations, but they cannot provide ETR data at regional and global scales. The remote sensing technology solves this limitation. On one hand, the remote sensing approach provides a synoptic view at regular time intervals avoiding extrapolation to large regions, and on the other hand, it is relatively inexpensive (e.g. Paruelo, 2008). Consequently, remote sensing ETR estimations have become, in the last three decades, the dominant approach both regionally and globally (Bastiaanssen et al. 1998; Di Bella et al. 2000, 2019; Cleugh et al. 2007; Mu et al. 2007; Leuning et al. 2008; Yang and Shang, 2013; Zhang et al. 2019; Bhattarai and Wagle, 2021).

In Uruguay, there are several attempts to quantify the ETR through different approaches (Giménez and García Petillo, 2011; Munka et al. 2013; Berger et al. 2015; Otero et al. 2015; Silveira et al. 2016; INIA-GRAS, 2022). In general, the studies focused on evaluating the ETR dynamics over time with data from a unique source or product. However, assessments related to the performance of the estimates of different sources/products, particularly from remote sensing, are still lacking. The only reported work compares the ETR derived from the MODIS product (MOD16A2) with three techniques: a water balance model, the Soil & Water Assessment Tool (SWAT) and an Eddy Covariance Flux tower (Navas et al. 2021). However, this work doesn’t consider inter-annual variations because its only analyse one year (Feb-2011 to May-2012). The main objectives of this article were: a) to evaluate the performance of different spatial explicit approaches to estimate real evapotranspiration, and b) to estimate and analyse (in a qualitative way) the variability in water yield derived from the different ETR sources/products for three climatically contrasting years (dry, average, and wet). For that, we use four remote sensing ETR products, with different spatial and temporal resolutions, and two water balance models at two scales, national and micro-watershed levels.

2. Methods

2.1. Study area

The study area includes the entire territory of Uruguay, which is located in the south-eastern South America between latitude 30-35 ° S and longitude 53- 58 ° W (Figure 1). The climate is temperate, with a mean-annual temperature of 17.5°C and a mean-annual precipitation of 1350 $mm.y^{-1}$ (INUMET, 2022). Temperature is highly seasonal, reaching maximums of 28°C in summer months (January) and minimums of 6°C in winter months (July). Precipitation is evenly distributed during the year, but with a high inter-annual variability ranging from 700 mm recorded in the driest year (1989) to 2000 mm recorded in the wettest year (2002) (INUMET, 2022). The country is dominated by rolling plains, with very smooth slopes, except in the eastern region (called eastern hills) (Panario et al. 2014).

Uruguay is entirely included in the “Campos” region of the Rio de la Plata Grasslands (Soriano et al. 1991, Paruelo et al. 2007; Oyarzabal et al. 2020). Grasslands represent the dominant vegetation type covering approximately 55% of the land surface (Baeza et al. 2022) and are commonly used for cattle and sheep production, the main economic activity in Uruguay (Gutiérrez et al. 2020). Also, there are two other important land-uses for the Uruguayan economy: croplands (mainly soybean) and exotic tree plantations (*Eucalyptus* and *Pinus*).

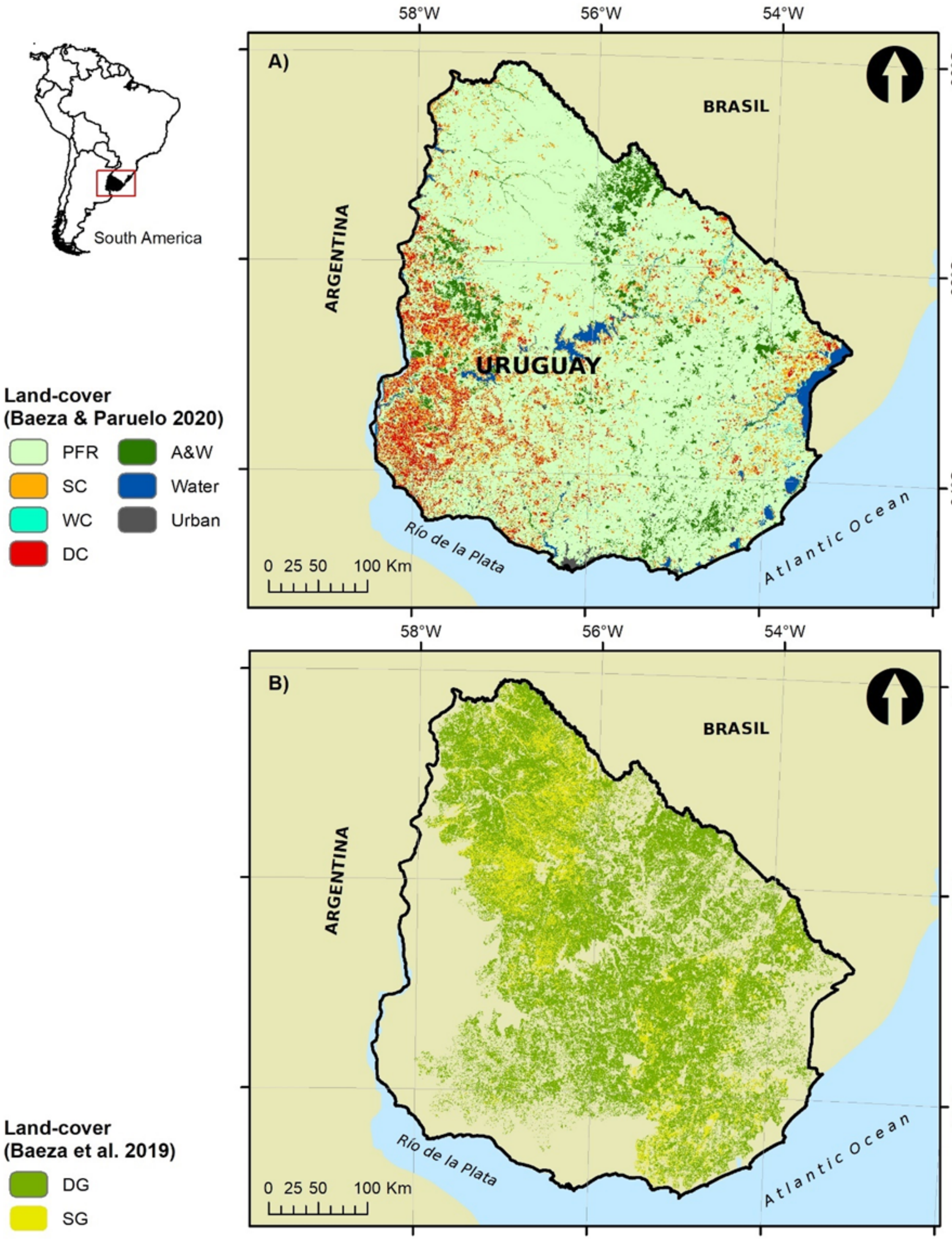

Figure 1: Location of the Uruguayan territory in South America. A) Land-cover map for 2012/2013 (see Baeza and Paruelo, 2020 for more details). PFR: Perennial Forage Resources, SC: Summer Crops, WC: Winter Crops, DC: Double Crops, A&W: Afforestation's and Woodland. B) Grassland

communities land-cover map (see Baeza et al. 2019 for more details). SG: Spercely-grasslands, DG: Densely-grasslands.

2.2. *Evapotranspiration products used in the performance evaluation.*

The performance evaluation of remote sensing and water yield based ETR products was carried out based on their ability to differentiate land-covers, their spatial and temporal resolution, their degree of coupling with NDVI and precipitation, and with ETR estimates based on field data.

2.2.1.Remote Sensing evapotranspiration products

2.2.1.1. PMLv2 product

The Penman–Monteith–Leuning model in its second version (v2) was developed by coupling a photosynthesis model (Farquha et al. 1980) and a canopy stomatal conductance model (Yu et al. 2004) with the Penman–Monteith energy balance equation (Monteith, 1965) to jointly estimate gross primary productivity and terrestrial ETR (Zhang et al. 2019). This model assumes that total ETR is the sum of evaporation from the soil (Es), transpiration from the plant canopy (Ec), and evaporation of precipitation intercepted by the vegetation (Ei) (Equation 1). PMLv2 produces an 8-day composite product at 500-meter for the 2003-2017 period (Table 1).

$$ETR = E_s + E_c + E_i \qquad \text{(Eq 1)}$$

The PMLv2 model was built using Google Earth Engine (Gorelick et al. 2017) and takes MODIS data (leaf area index, albedo, and emissivity) together with GLDAS meteorological forcing data as model inputs (see more details in Zhang et al. 2019). This product decomposes the ETR values in each component (Es, Ec and Ei) separately. In this article, we evaluate two combinations: a) the sum of Ec and Ei (hereafter called *PMLv2 (Ec+Ei)*) and the sum of Ec, Ei, and Es components (hereafter called *PMLv2*).

2.2.1.2. MOD16A2 product

The MOD16A2 (Collection 6, hereafter *MODIS*) provides global terrestrial ETR using a modified Penman-Monteith method (Mu et al. 2011). This ETR product used remote sensing data from the Moderate Resolution Imaging Spectroradiometer (vegetation property dynamics, albedo, and land-cover) and the global reanalysis from the Modern-Era Retrospective Analysis for Research and Applications (MERRA; Rienecker et al. 2011). This ETR dataset is an 8-day composite product at 500-meter from 2001 to the present (Table 1; Running et al. 2017).

The total daily ETR corresponds to the sum of the evaporation from the wet canopy surface (E_{Wet}), the transpiration from the dry canopy surface (T_{Dry}), and the evaporation from the soil surface (E_{Soil}) (Equation 2). Contrary to the *PMLv2* product, MOD16A2 does not provide the ETR components separately.

$$ETR = E_{Wet} + T_{Dry} + E_{Soil} \qquad \text{(Eq. 2)}$$

2.2.1.3. INTA-SEPA product

The National Institute of Agricultural Technology of Argentina (INTA), through the "Agricultural Production Monitoring" initiative (hereafter *INTA-SEPA*), provides ETR estimations based on a model generated by Di Bella et al. (2000) (Equation 3). This model is based on both thermal infrared (surface temperature - T_s) and vegetation index (Normalized Difference Vegetation Index, NDVI) data obtained from the Advanced Very High-Resolution Radiometer (AVHRR) sensor on board the National Oceanic and Atmospheric Administration (NOAA) satellite. This product was developed for the Argentine Pampas and provides ETR estimations, with a 1x1 km^2 spatial and 10-days temporal resolutions, for the 2002-2018 period (Table 1; see more details in http://sepa.inta.gob.ar/productos/agrometeorologia/et_10d/).

$$ETR = -88.3439 + 1.77636 * Ts + 286.406 * NDVI \qquad \text{(Eq. 3)}$$

2.2.1.4. Landsat product

Jackson et al. (1977) proposed the commonly called “Jackson Simplified Method” to estimate daily ETR using surface radiant temperature measurements (Equation 4). This method can be applied for Landsat images (30-meter and 16-day; Table 1) and calculates daily ETR considering the net radiation received by the surface and its temperature difference with the surrounding air mass equation (Jackson et al. 1977)

$$ETR = Rn - B(Ts - Ta)^n - G \qquad \text{(Eq. 4)}$$

where ETR (mm day^{-1}) and Rn (mm day^{-1}) are, respectively, the integrated actual ETR and net radiation over a 24 h period, Ts (K) is the surface radiant temperature, Ta (K) is the 1.5 m air temperature above ground level, G (mm day^{-1}) is the soil surface energy flux, and B (mm day^{-1} K^{-1}) and n are parameters that vary with vegetation activity estimated from the NDVI.

Although this method is simple, it also has a strong physical basis and has been successfully applied for different vegetation types (Caselles et al. 1998; Sanchez and Caselles, 2004; Nosetto et al. 2005; 2012; Milkovic et al. 2019). In this work, we used 11 Landsat-7 images and 1 Landsat-8 image (path/rows: 223/83; 223/84; 224/84; 225/82 and 224/82) for the 2012-2013 period to estimate ETR following the Jackson Simplified Method. Images were provided by the USGS (https://earthexplorer.usgs.gov/) and cover 65% of the Uruguayan territory. Images were acquired between 12:05 and 12:20 hours (local time) on 27/10/2012, 3/11/2012, 5/11/2012, 7/2/2013, 4/3/2013, 11/3/2013, 13/3/2013, 27/3/2013 and 13/4/2013. Non-thermal bands were corrected using the Landsat Ecosystem Disturbance Adaptive Processing System (LEDAPS) atmospheric correction described by Masek et al. (2012), and the thermal bands were corrected using the mono-window algorithm proposed by Qin et al. (2001). Also, images were filtered by its quality band ("bqa") generating products free of clouds, shadows, and water. Meteorological data, required to estimate ETR, were derived from six meteorological stations (INIA Tacuarembó, INIA Salto Grande, INIA Treinta y Tres, INIA Glencoe, INIA La Estanzuela, INIA Las Brujas). For more details about the Jackson Simplified Method ETR estimation (hereafter *Landsat*) see supplementary material 1.

2.2.2. Water balance evapotranspiration products

2.2.2.1. INIA-GRAS

The National Institute of Agricultural Research of Uruguay, through the Information Systems and Digital Transformation Area (hereafter *INIA-GRAS*), provides ETR estimations based on a water balance model for the soils of Uruguay. This model is calculated at the national level and a daily step, for a grid with cells of approximately 30 x 30 km^2 (Table 1; see Figure S1 in supplementary material 2). The input variables of the model are the water-holding capacity of the soil (it considers the maximum amount of water that the soil can store between field capacity and permanent wilting point), the effective precipitation and the potential evapotranspiration (Penman method). For each grid cell, the water-holding capacity is calculated as a weighted average value of the Potentially Available Soil Water Net (APDN) of the Soil Units that are within each cell. For the agrometeorological variables (potential evapotranspiration and effective precipitation), a network of meteorological stations throughout the Uruguayan territory (INIA and INUMET) is used and the average daily value is estimated for each cell using the interpolation method (see more details in http://www.inia.uy/GRAS).

2.2.2.2. Silveira et al. (2016)

Silveira et al. (2016) estimated the ETR based on the water balance (Equation 6) of two micro-watersheds with similar geomorphological and edaphic characteristics: a) Don Tomas (2.12 km^2) used for active forestry with *Eucalyptus globulus* since 1998 and b) La Cantera (1.2 km^2) used for cattle ranching based on native grasslands (see Figure S2 in supplementary material 2). To carry out the water balance in the two micro-watersheds, Silveira et al. (2016) used monthly field data information (aggregated seasonally and annually) of precipitation, soil moisture and runoff from October 2006 to September 2009 (Table 1).

The ETR, derived from the water balance, was calculated as:

$$ETR = PPT - Q_s \pm \Delta S \pm \Delta GW \qquad \text{(Eq. 5)}$$

where ETR is the actual evapotranspiration, PPT is the incident precipitation, Q_s is the stream discharge at the watershed outlet, ΔS is the change in soil water storage, and ΔGW is the change in groundwater storage.

Table 1: Characteristics of remote sensing and water yield evapotranspiration (ETR) products

	ETR product	Spatial resolution (km)	Temporal resolution (days)	Period	Scale	Reference
Remote sensing products	PMLv2	0.5	8	2003-2017	Global	Zhang et al. 2019
	MOD16A2	0.5	8	2001-present	Global	Running et al. 2017
	INTA-SEPA	1	10	2002-2018	Regional	Di Bella et al. 2000
	Landsat	0.03	16	1985-present	Local	Jackson et al. 1977
Water balance products	INIA-GRAS	30	1	2003-present	National	INIA Uruguay
	Silveira et al.	-	30	2006-2009	Watershed	Silveira et al. 2016

2.3. *Precipitation data*

Precipitation data were obtained from the Climate Hazards Group InfraRed Precipitation with Station product (CHIRPS; Funk et al. 2015). This dataset is available in Google Earth Engine and provides daily precipitation data estimations (mm/day) with a spatial resolution of 0.05° x 0.05° (5 ×

5 km^2, approximately) since 1981. The precipitation values were converted into accumulated monthly (mm/month) and annual (mm/year) precipitation for the 2002-2017 period.

2.4. *NDVI data*

NDVI data were obtained from the Mod13Q1 product (collection 6 of MODIS). These images have a spatial resolution of 250 m (~6 ha per pixel) and a temporal resolution of 16 days. Each NDVI image was filtered using its associated "per pixel" quality band (Roy et al. 2002). Pixels that did not have the highest quality were discarded and their values replaced by simple linear interpolation from the previous and the following dates of the same pixel. NDVI values were used at 16-d step and mean annual scale for the 2003-2017 period.

2.5. *Land-cover maps*

To characterize the ETR and NDVI seasonal dynamic, we used two land-cover maps with different but complementary conceptual resolutions (Figure 1). The first one, used as the base, corresponds to the 2012-2013 period, and discriminates between 7 categories: perennial forage resources, summer crops, winter crops, double crops, afforestation and woodland, water, and urban. It was built using simple but exhaustive classifications based on a time series of MODIS NDVI satellite images (250-meter) and decision trees classifiers (for more details see Baeza and Paruelo et al., 2020). The second one corresponds to the 2016 year and was used to disaggregate the class perennial forage resources into two types of native grasslands called "Densely vegetated grasslands" and "Sparsely vegetated grasslands". This map was built using Landsat 8 images and supervised classifications (for more details see Baeza et al. 2019).

2.6. *Water Yield estimation*

We calculated the daily Water Yield (WY, Equation 6) at a micro-watersheds level (n= 1426, 125 km^2 average; *Ministerio de Ambiente*, 2022; https://www.ambiente.gub.uy/visualizador/index.php?

vis=sig) for the period 2003-2017). Here, we only show the WY for three climatically contrasting years: wet (2014 with an average of 1800 ± 500 mm), average (2010 with an average of 1370 ± 450 mm), and dry (2008 with an average of 840 ± 415 mm). We used data from all remote sensing ETR products (except Landsat and INIA-GRAS due to its temporal and spatial resolution), daily precipitation and soil water content for the 0-100 cm profile.

Water yield was calculated as:

$$WY = \Delta S_{t-1} + PPT_{t0} - ETR_{t0} - FC_{t0} \qquad \text{(Eq. 6)}$$

where WY is the water yield (mm/d), ΔS is the available water in the soil, PPT is the precipitation (mm/d), ETR is the real evapotranspiration (mm/d) derived from the different data sources, FC is the field capacity up to 1-meter derived from the Hengl and Gupta (2019) product, and t0 y t-1 represent the time period estimations. We consider 01/01/2003 as the initial date of FC_{t0} as it was preceded by a particularly wet month that allowed us to assume that the soil was at field capacity (230 mm in December 2002 representing 140 % more than the historical average). The initial FC value was subtracted from the PPT - ET balance and the WY equation was iterated at a daily step for the 2003-2017 period. All pure pixels within the micro-watersheds were averaged. This analysis, based on a qualitative approach, takes a step further in evaluating the performance of ETR products, allowing for an applied approach to water management in micro watersheds.

2.7. *Data analysis*

We analysed the relationship between the different ETR products and the a) annual precipitation and b) annual NDVI using linear regressions for the period 2003-2017. For this purpose, and to make the different spatial resolutions of the products compatible, we calculated the average of each variable (dependent and independent) for the 30 x 30 km grid (n= 102), on which *INIA-GRAS* provides the ETR estimations. Grids with more than 10 % of water bodies were discarded. To characterize the temporal dynamics of NDVI and ETR of each product for different land-covers, we selected "pure" pixels from each land-cover (water and urban classes were excluded). We extracted the NDVI values from the MOD13Q1 product and the ETR values from PMLv2 (*PMLv2 (Ec+Ei*) and *PMLv2 (Ec+Ei+Es)*), *MODIS* and *INTA-SEPA* products. We excluded for this analysis the *INIA-GRAS* ETR dataset due to its spatial resolution (30x30 km). The relationship between the different ETR products and the Jackson Simplified Method (*Landsat*) was analysed using linear regressions. We used the same pure pixel and selected those that intersected with the Landsat scenes (n= 122.000 for *MODIS* and *PMLv2* products, and n= 117.000 for *INTA-SEPA* product). We considered the median of each date and ETR product. Finally, the relationship between the different ETR products (except *INIA-GRAS*) and the ETR calculated from the water balance (proposed by *Silveira et al.* (2016)) was analysed using linear regression models. All pure micro-watershed pixels and ETR data accumulated every six months were used in the model. Statistical analyses were performed in R Core Team (2021)

For the ETR products comparison (*PMLv2, PMLv2 (Ec+Ei), MODIS, INTA-SEPA and INIA-GRAS*) we considered six criteria: 1) the temporal and 2) spatial resolution, 3) the correlation (expressed as the Pearson correlation coefficient) with the annual NDVI and 4) the annual precipitation, 5) the slope of the linear model with the *Silveira et al.* (2016) water balance and 6) the slope of the linear model with the Jackson Simplified Method (*Landsat*). Criteria 3 to 6 represent different perspectives to evaluate the performance of the database. Each criterion was scaled to the range [0-1] to make them comparable, using the equation 7:

$$X_i \ scaled = (X_i - X_{min})/(X_{max} - X_{min}) \quad \text{(Eq. 7)}$$

Where X_i *scaled* corresponds to the scaled value of criterion *X* for the ETR product *i*, X_i is the value taken by criterion *X* for the ETR product *i*, X_{min} is the minimum value taken by criterion *X* among all the ETR products and $X_{máx}$ is the maximum value taken by criterion *X*.

3. Results

The fitted models and the Pearson correlation coefficients obtained between the remote sensing products (excluding Jackson Simplified Method due to its low temporal resolution) and the annual NDVI and precipitation, for the period 2003-2017, showed contrasting results (Figure 2 and Table S1 in supplementary material 3). There is a significant, positive, and linear correlation for models fitted for *PMLv2(Ec+Ei)*, *MODIS* and *INIA-GRAS* products. The highest Pearson correlation coefficient, for both NDVI and PPT, was observed for the model fitted with *MODIS* (r=0.84 and r=0.72, respectively), followed by *INIA-GRAS* (r=0.64 and r= 0.59, respectively) and *PMLv2(Ec+Ei)* (r=0.77 and r= 0.56, respectively). On the other hand, the models fitted with *INTA-SEPA* and *PMLv2* products showed a non-significant fit (p>0.05).

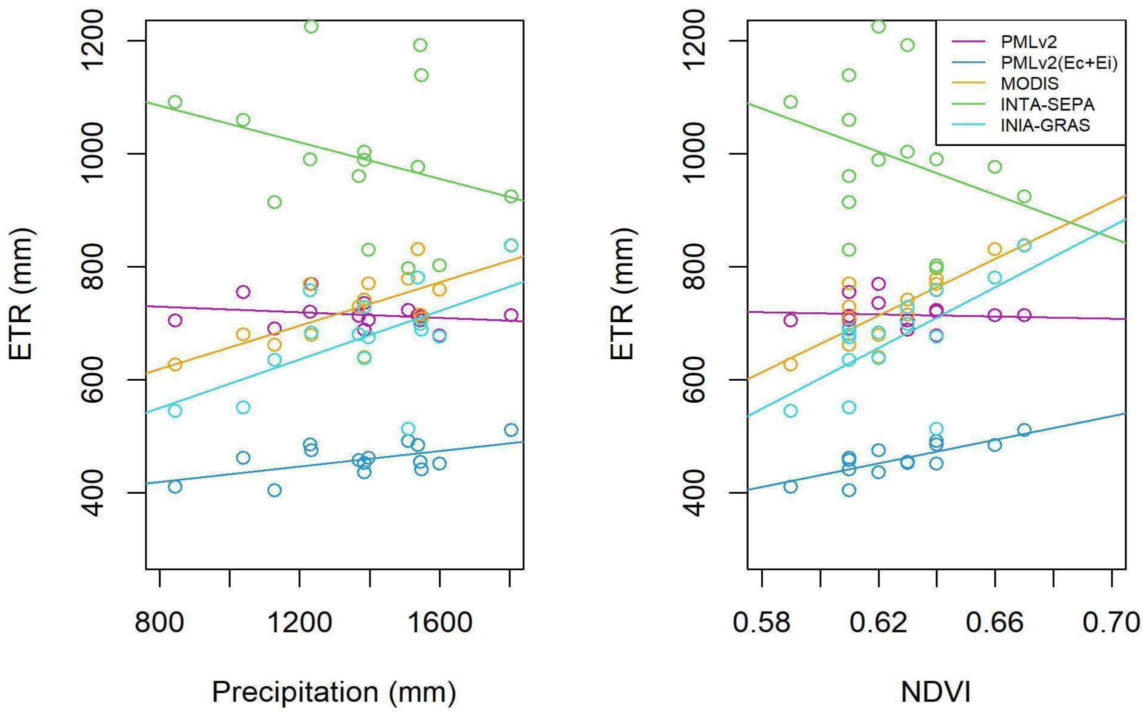

Figure 2: Fitted models between the annual evapotranspiration (2003-2017) for each product (*PMLv2, PMLv2(Ec+Ei), MODIS, INTA-SEPA* and *INIA-GRAS*) and a) (left) the annual precipitation and b) (right) the annual normalized difference vegetation index.

All ETR products evaluated and the NDVI showed, for all land-covers, a strong seasonality with maximum values in summer, minimum values in winter and intermediate values in autumn and spring months (Figure 3). Also, differences among land-covers were higher in summer and lower in winter months. Differences between land-covers were maximum in *MODIS* and *PMLv2(Ec+Ei)* products and minimum for *PMLv2* and *INTA-SEPA* products (see results for annual estimates in Figure S3 in supplementary material 2). Furthermore, the ETR estimates from the *INTA-SEPA* model showed an irregular temporal dynamic with curves exhibiting very pronounced peaks and valleys. Afforestation and woodland showed the highest ETR values for almost the whole year for the *MODIS* and *PMLv2(Ec+Ei)* products (3 and 2 mm, respectively). This pattern is consistent with the annual dynamics of NDVI, where this cover not only showed the highest values throughout the year (an average of 0.8) but was also the class with the lowest intra-annual variability (cv=3.8%). In terms of agricultural classes, double crops showed a clear bimodal pattern in the *PMLv2(Ec+Ei)* and *MODIS* products (this pattern is more clear for the *MODIS* product). Also, this pattern was observed in the NDVI dynamic with maximum peaks in spring and summer, associated with double crop sequences. Summer crops showed a unimodal pattern with maximum values of ETR (*PMLv2(Ec+Ei)* and *MODIS*) and NDVI in summer (3.5 mm and 0.75 approximately, respectively). Winter crops showed two peaks (spring and late summer) in the *MODIS* product and a single peak in summer for the rest of the ETR products. NDVI for winter crops was characterised by high values in both spring and autumn. On the other hand, densely-vegetated grasslands showed, for all months of the year, higher NDVI and ETR values than sparsely-vegetated grasslands, particularly for *MODIS* and *PMLv2(Ec+Ei)* products. In both grassland types, and for all ETR products, the maximum values were reached in spring-summer and minimum in winter. This pattern also is consistent with the annual dynamics of NDVI.

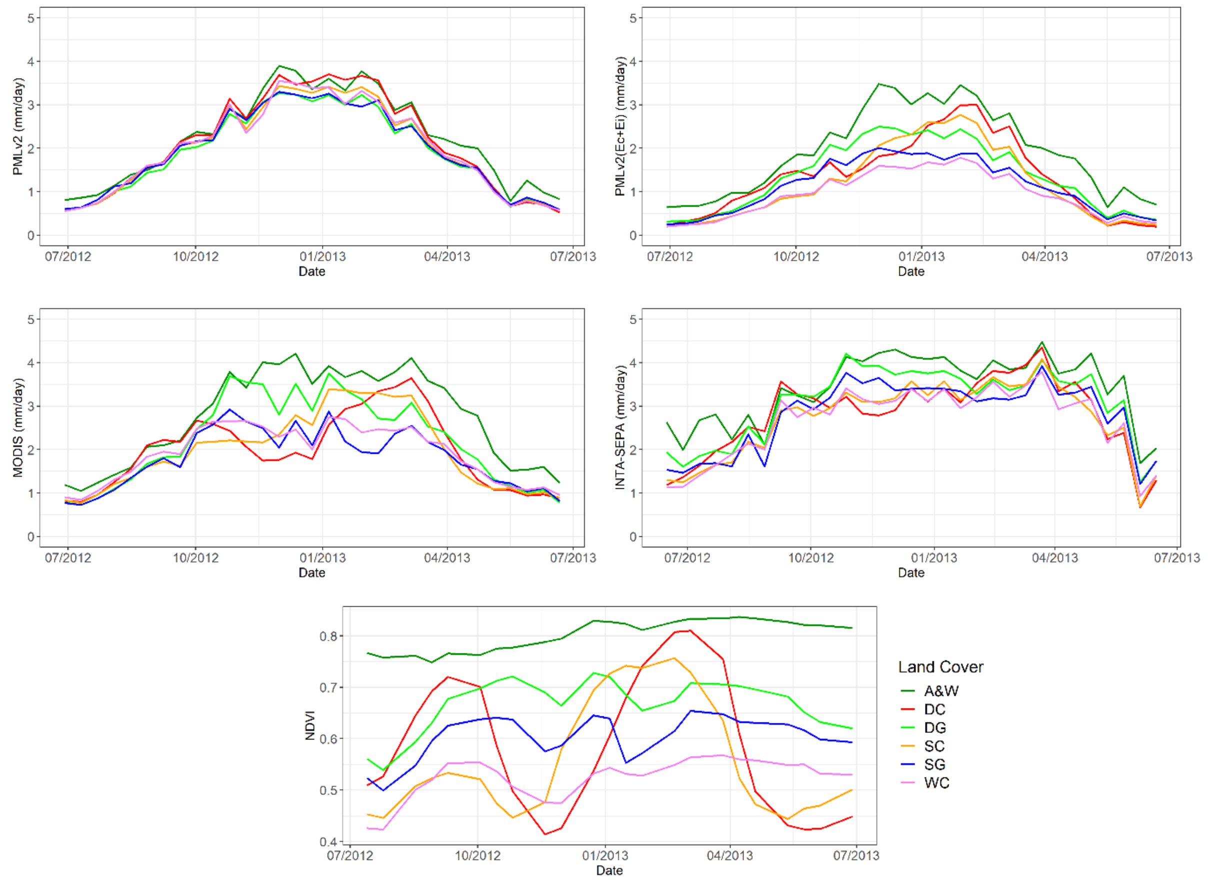

Figure 3: Evapotranspiration products and normalized difference vegetation index (NDVI) seasonal dynamic for different land-covers classes in the 2012-2013 period. In: 8-d intervals for *PMLv2* and *MODIS* products, 10-d intervals for *INTA-SEPA* product and 16-d intervals for NDVI-MODIS product. Different colours represent land-covers: SG: Sparsely-vegetated grassland; DG: Densely-vegetated grassland; A&W: Afforestation and Woodland; DC: Double Crops; WC: Winter Crops; SC: Summer Crops.

The fitted models between the *PMLv2, PMLv2(EC+Ei), MODIS* and *INTA-SEPA* products (*INIA-GRAS* product was excluded due to its spatial resolution) and the Simplified Jackson Method (derived from Landsat-7 and 8 images) showed significant, linear, and positive correlations (Figure 4). Fitted models differed mainly in terms of the slope and the Pearson correlation coefficient. The model with the highest Pearson correlation coefficient was *PMLv2(Ec+Ei)* (r= 0.60, p<0.001), followed by *MODIS* (r= 0.54, p<0.001). *INTA-SEPA* and *PMLv2* showed the lowest Pearson correlation coefficient (r= 0.36, p<0.05 and r= 0.34, p<0.05, respectively). The slope of all models showed a value less than 1, with extremes of 0.53 and 0.17 for *MODIS* and *INTA-SEPA* respectively. In general terms, the different land-covers maintained the same distribution pattern for the several fitted models.

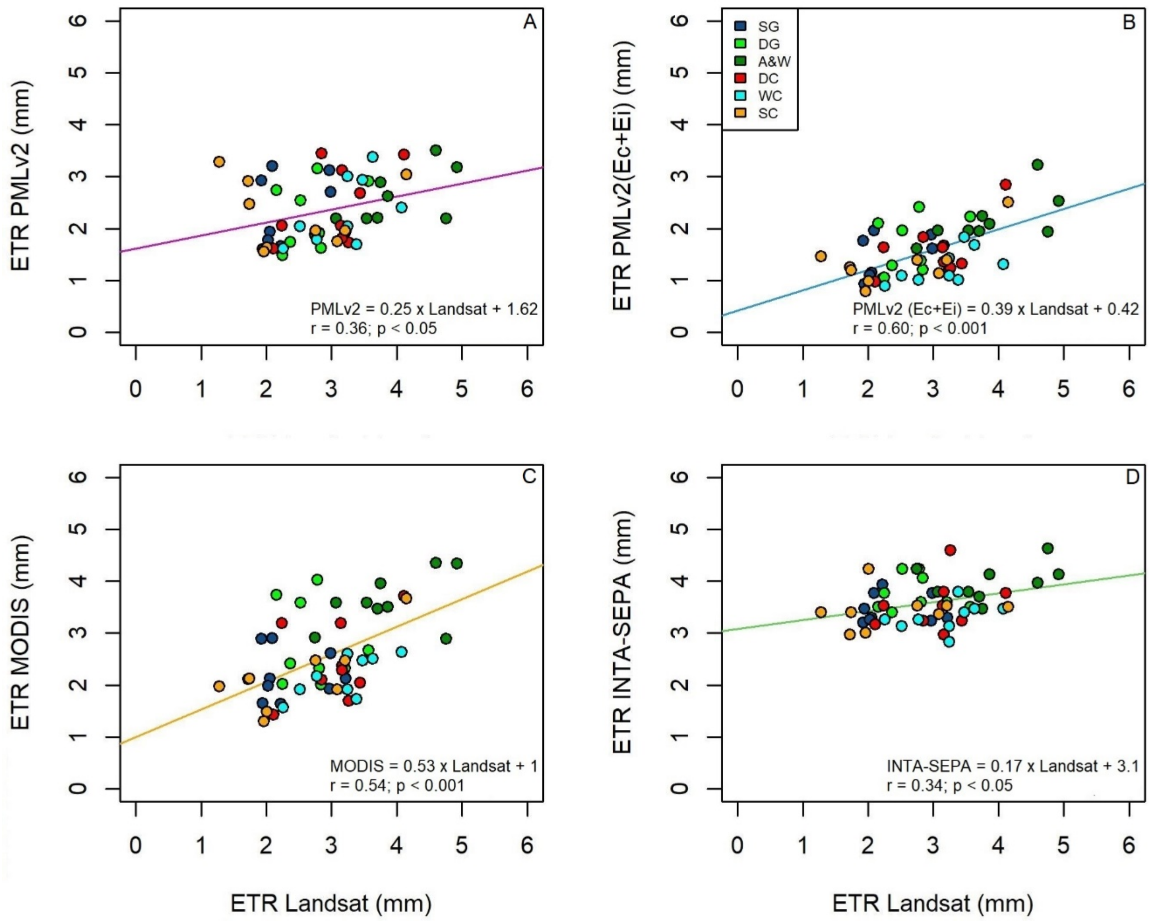

Figure 4: Fitted linear regression models between the evapotranspiration of: A) *PMLv2*, B) *PMLv2(Ec+Ei)*, C) *MODIS*, D) *INTA-SEPA* and the evapotranspiration estimated from the Simplified Jackson Method (derived from *Landsat* data). Different colours represent land-covers: SG: Sparsely-vegetated grassland; DG: Densely-vegetated grassland; A&W: Afforestation and Woodland; DC: Double Crops; WC: Winter Crops; SC: Summer Crops.

ETR derived from *PMLv2, PMLv2(EC+Ei), MODIS* and *INTA-SEPA* products showed a linear and positive correlation (p<0.001) with water balance estimates of ETR in the two experimental watersheds (Figure 5). In general terms, all models showed a high Pearson correlation coefficient, surpassing 75 % of the variance explained. In terms of slope, all models presented values greater than 1. The model closest to this value was *PMLv2* (slope=1.31) while the model furthest away was INTA-SEPA (slope=1.78). Additionally, all fitted models showed the same distribution pattern for forestations and grasslands.

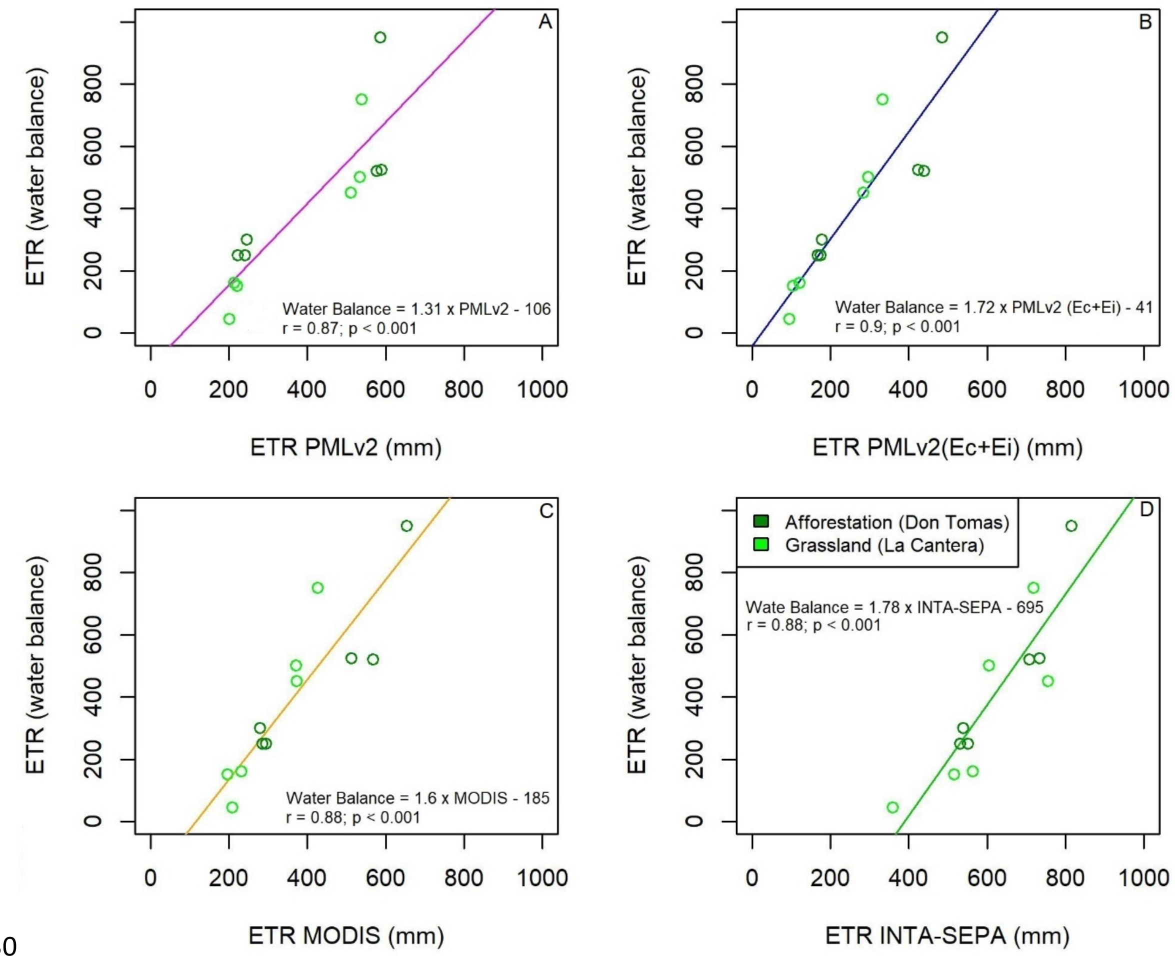

Figure 5: Fitted linear regression models between ETR products: A) *PMLv2*, B) *PMLv2(Ec+Ei)*, C) *MODIS*, D) *INTA-SEPA* and the ETR estimated from the water balance proposed by Silveira et al. (2016). Different colours represent land-covers in each watershed: afforestation (Don Tomas watershed) and grasslands (La Cantera watershed).

Radar plots describes the ETR estimation performance of the different products (both based on remotely sensed and water balance data) for the 6 criteria (Figure 6). The results show important differences between the performances of the different ETR products analysed. On one hand, the *INTA-SEPA* was the product with the lowest relative performance in 5 of the 6 criteria analysed. The spatial resolution of this product (1000 m) is the only criterion that was weighted positively. In the opposite case, the *MODIS* and *PMLv2(EC+Ei)* products showed high relative performances in 4 of the 6 criteria, including spatial and temporal resolution (500 m and 8-d), correlation with precipitation and NDVI (up to 60%) and the ability to discriminate between land-covers (slopes>=0.39). The *INIA-GRAS* product showed well results in 3 of the 6 criteria, with temporal resolution (1-d), and correlation with NDVI and precipitation (r=0.64 and r= 0.59, respectively). Finally, the *PMLv2* product stood out in 2 of the 6 criteria, its high spatial resolution (500m) and the similarity with the ETR estimated from the water balance for the two micro-watersheds (slope=1.31).

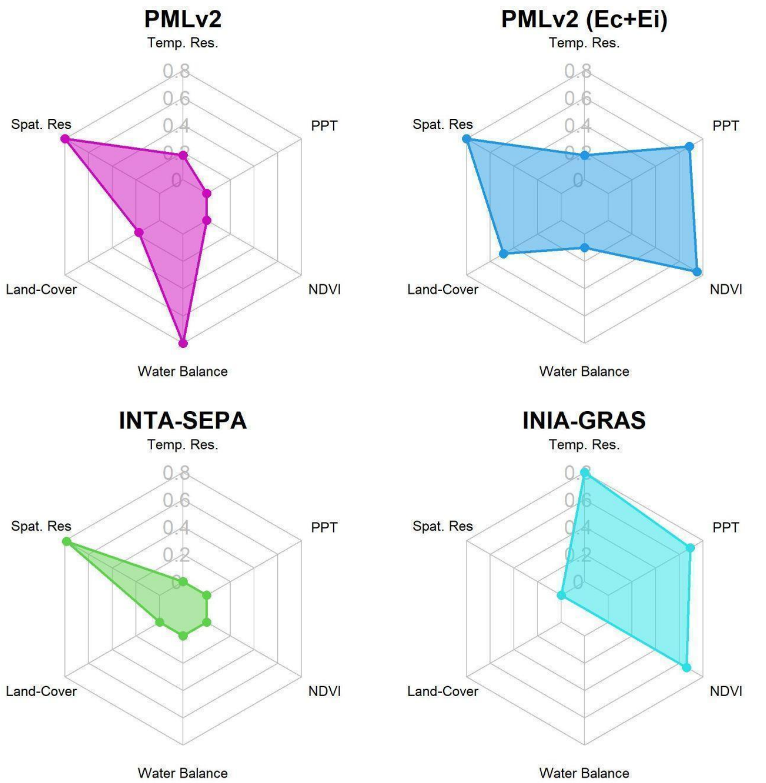

Figure 6: Radar plots for each evapotranspiration product (*PMLv2*, *PMLv2(Ec+Ei)*, *MODIS*, *INTA-SEPA*, *INIA-GRAS*) evaluated on six criterions. All the criterions were scaled from 0 to 1. Criterions: 1. Temp.

Res. (temporal resolution); 2. PPT (precipitation); 3. NDVI (normalized difference vegetation index); 4. Water Balance; 5. Land-Cover (land-cover differentiation); 6. Spat. Res. (spatial resolution).

Water yield estimates, derived from the use of the different ETR products (except for *INIA-GRAS* due the low spatial resolution) (Figure 7), showed similar spatial patterns with Pearson correlation coefficients ranging from 0.784 to 0.959 (Figure S4 in supplementary material 2). However, the magnitude and spatial pattern of WY estimates differed among products. Regarding temporal changes, all evapotranspiration products captured changes in water yield among contrasting years in terms of total precipitation. A clear increasing WY pattern from SW to NE can be observed, with the highest values for estimates derived from the *PMLv2(Ec+Ei)* product. On the other hand, the comparison of the water yield for the same year and between evapotranspiration products showed important differences. In the case of the dry year (2008), the *INTA-SEPA* model characterized the entire Uruguayan territory within the category with the lowest values (a mean annual of 67 mm). On the other hand, both *MODIS* and *PMLv2* showed greater heterogeneity and a very similar spatial distribution (mean annual of 221 and 196 mm, respectively). *PMLv2(Ec+Ei)* showed even greater heterogeneity, showing a different spatial pattern than the rest of the products (mean annual of 431 mm). For the year with average precipitation (2010), we also found contrasting differences between the WY estimates. The estimates derived from the *INTA-SEPA* product showed a large part of the territory (more than 50 %) with values between 300 and 600 mm, and even some SW micro-watershed showed values between 0 and 300 mm (mean annual of 537 mm). *MODIS* and *PMLv2* showed a similar pattern, with values between 300 and 600 mm in the SW, NW and E of the Uruguayan territory (mean annual of 668 and 739 mm, respectively). *PMLv2(EC+Ei)* was characterized by higher values ranging from 1000 to 1200, in most of the analysed territory. Finally, for the wet year (2014), the differences were accentuated, particularly in the mean annual WY estimated from *PMLv2(Ec+Ei)* (1230 mm) which showed between 30 and 50% more WY than the rest of the estimates.

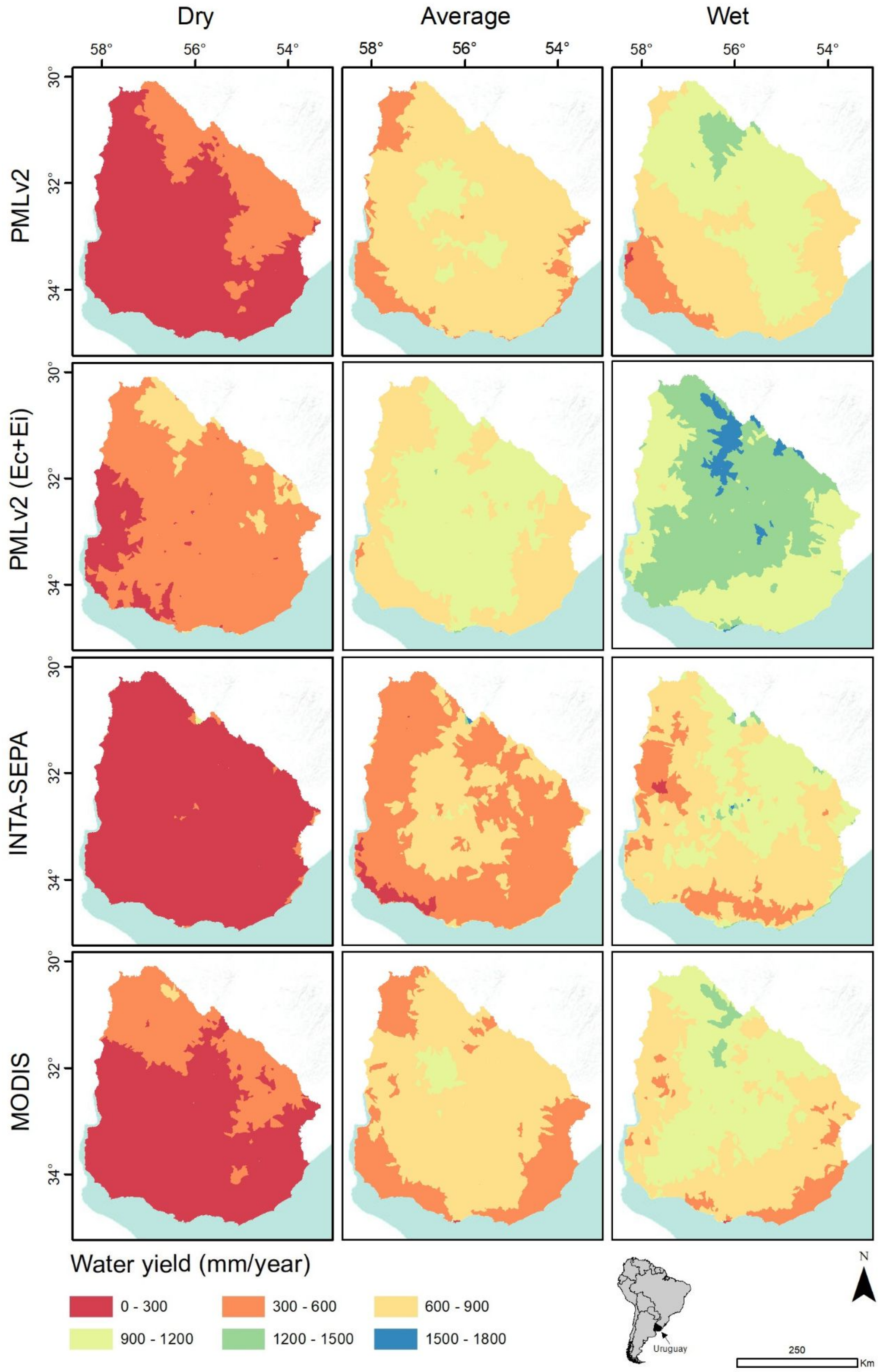

Figure 7: Water yield maps estimated from the different remote sensing evapotranspiration products at the micro-watershed scale in climatically contrasting years: Dry: 2008 (precipitation: 840 mm); Average: 2010 (precipitation: 1370 mm); Wet: 2014 (precipitation: 1800 mm).

4. Discussion

This study describes and compares the inter-annual and seasonal annual dynamic of four remote sensing ETR products (*PMLv2* with three and two components, *MODIS*, *INTA-SEPA*) and analyses their performance in terms of 6 criteria (correlation with the annual productivity and precipitation, spatial and temporal resolution, land-cover differentiation, and correlation with ETR water balance estimates). Also, this study describes the spatial and temporal variability of the WY derived from each remote sensing ETR product. It is important to mention that this work represents an intercomparison of ETR estimation models in Uruguay. Strictly, this work does not represent a validation of the models, except for their comparison with micro-watershed data, which cover a small area in the Uruguayan territory. Clearly, our results show important differences between the ETR estimation products that resulted in important differences in WY estimation. Among the best performing ETR products, based on the 6 criteria analysed, *MODIS* and *PMLv2(Ec+Ei)* stand out. Both products have high spatial (500-m) and temporal (8-d) resolution, capture seasonal differences between land-covers and showed positive and high correlations with the annual productivity and precipitation. Our results are in line with several global and regional studies that have shown that both *MODIS* and *PMLv2* products generate good estimates of actual evapotranspiration (Guerschman et al. 2009; Velpuri et al. 2013; Aguilar et al. 2018, Faisol et al. 2019; Xu et al. 2019; Chao et al. 2021; Navas et al. 2021).

The absolute value of ETR derived from each product showed profound differences. These differences were reflected both in the monthly ETR dynamics of the different land-covers as well as in the comparison with the data provided by the simplified Jackson model (based on Landsat data) and its correlation with the annual productivity and precipitation. Regarding the comparison with the monthly dynamics of the NDVI for 2012/2013, the ETR products showed a marked difference. A priori, what we expected was that all models would follow the monthly NDVI dynamics, i.e., copy the same monthly pattern for the different land-covers. This is because, on the one hand, ETR is closely linked to C dynamics and Leaf Area Index (Cihlar et al. 1991; Chapin III et al. 2011) and on the other hand, all products consider, to some extent, vegetation aspects/properties (NDVI in the case of *INTA-SEPA* (Di Bella et al. 2000), or leaf area index in the case of *PLMv2* and *MODIS* (Mu et al. 2011; Zhang et al. 2019). Similarly, the correlation with the annual NDVI and precipitation (15 years, 2003-2017 period), for the whole Uruguay, showed clear differences between models, being in some cases, opposite to what was expected. For example, the *INTA-SEPA* and *PMLv2* (with its three components; Ec, Ei and Es) products showed no relationship with both variables.

In general terms, the intercomparison showed that the worst performing models were *PMLv2* and *INTA-SEPA*. Particularly, in the case of *PMLv2*, our results do not agree with those reported by Chao et al. (2021). These authors demonstrated that *PMLv2* is one of the best performing models in North America when compared to in-situ data based on water balance estimations. The differences found in this work could be associated with many factors, such as the forcing data (precipitation, air temperature, vapor pressure, shortwave downward radiation, longwave downward radiation, and wind speed), the parameters of each ETR algorithms or the nature of the algorithms themselves. In the case of *PMLv2*, the model assumes that all net radiation is decomposed into three components: Es, Ei and Ec, unfailingly giving values to one of these three fluxes (Zhang et al. 2019). When we compare separately *PMLv2* with three and two components, the absolute values increase drastically relative to *PMLv2(Ec+Ei)* and the differences, for example, in the intra-annual dynamics of ETR decrease between land-covers (all land-covers have a similar seasonal pattern without marked differences). We hypothesize that this could be associated with the fact that the Es flux simplifies the physical processes, contributing energy to the evaporation of soil water that is not part of the system (e.g surface and deep drainage). In fact, Zhang et al. (2019) propose that the Ec component is directly coupled with carbon assimilation and the other components, Es and Ei, may be indirectly linked with C as Es decreases and Ei increases associated with C, especially when the vegetation cover increases. On the other hand, the *INTA-SEPA* ETR product has several limitations. Clearly, this is the simplest model of this intercomparison that considers only NDVI and Ts, leaving out key variables that determine ETR, e.g., air temperature as a regulator of atmospheric water demand. It does not even consider net radiation, which has been shown to be the variable with the greatest relative weight, explaining 87% of the monthly variation in ETR (Fisher et al. 2009). Although the *INTA-SEPA* model presented good fits in its validation process (see more details in Di Bella et al. 2000), the product was validated for Argentina for a period with climatically average years. In the recent years that product has been updated and improved, both spatially and temporally, but it is only available since 2019 (Di Bella et al. 2019).

A strict validation of the analysed ETR products, based on two micro-watersheds, showed very good results for all models. The Pearson correlation coefficients were between 0.87 and 0.9. However, there were significant differences in the slopes. *MODIS* and *PMLv2* overestimated at values below 400 mm and underestimated at values above 400 mm. This is in agreement with Chang et al. (2018) where they found that the *MODIS* algorithm tended to underestimate ETR at high values and overestimate it at low values in the Tibetan Plateau, China. Also, Degano et al. (2021) in the Argentinean Pampas concluded that the *MODIS* product has a better performance in semi-arid areas than in humid areas. In such regions, the satellite product underestimates in the most stations, while, in semi-arid zones, the satellite values are close to ground measurements. Moreover, Navas et al. (2021) found in Uruguay better performances in wet season (particularly in autumn). In contrast, Chao et al. (2021) found in North America that *PMLv2* tends to overestimate at low values, adjust well at values between 400-600 and underestimate at medium and high values (600-1500). Furthermore, Chao et al., (2021) found for *MODIS* a systematic underestimation of the ETR in all ranges. *INTA-SEPA* and *PMLv2(Ec+Ei)* showed an underestimation and overestimation, respectively, over the whole range of values (0-1000 mm) and there are no studies that allow a comparison of these results. Overall, the differences found for the four models could be associated with the nature of the different algorithms, which some are based on NDVI and surface temperature such as Di Bella et al., (2000) and others on the Penman-Monteith method such as Mu et al. (2011) and Zhang et al. (2019) as well as the accuracy of in-situ observations (Chao et al. 2021).

5. Conclusions

In this study, we generated an intercomparison of four remote sensing ETR products based on 6 criteria and evaluated the accuracy of its estimations based on data derived from a simple water balance in two micro-watersheds. Also, based on the ETR products, we estimated the water yield for climatically contrasting years (wet, dry, and average). Our results suggest that *MODIS* and *PMLv2 (Ec+Ei)* remote sensing products demonstrated better performances on the 6 criteria analysed for Uruguay. The *INIA-GRAS* ETR water balance ETR product has shown to be a good reference product at the regional level while *PMLv2* and *INTA-SEPA* were the worst-performing models. The differences found between products have direct implications on the WY estimates, not only in the quantity but also in the spatial pattern. Accurate quantification of WY is not a simple matter, and the international literature has found, for the same remote sensing product, important differences in its performance between years and regions, possibly associated with model parameters, climatic and topographic conditions of the areas of interest, and aspects related to scale, among other factors. In this work, although two products were the best performing, they leave open questions for future improvements. In that sense, future research should address these aspects to expand their applications for understanding hydrological and ecological processes, global climate change research, agricultural drought detection and mitigation, and water resource management (Allen et al. 2005; Trenberth et al. 2009).

6. Acknowledge

The authors thanks Patricio Oricchio (Instituto de Clima y Agua – CIRN INTA Castelar) for the information provided. This research was funded by the FMV - ANII project (FMV_3_2020_1_162279) and INIA.

7. Author contributions

Conceptualization: FG, GCS and JMP; Data curation: FG, GCS and GT; Formal analysis: FG and GCS; Funding acquisition: FG; Investigation: FG, GCS and JMP; Methodology: FG, GCS and JMP; Validation: FG, GCS and JMP; Visualization: FG and GCS; Writing - original draft: FG; Writing - review & editing: FG, GCS, JMP, CD, GT.

8. References

Aguilar, A. L., Flores, H., Crespo, G., Marín, M. I., Campos, I., Calera, A., 2018. Performance assessment of MOD16 in evapotranspiration evaluation in Northwestern Mexico. Water. 10, 901. https://doi.org/10.3390/w10070901

Allen, R. G., Clemmens, A. J., Burt, C. M., Solomon, K., O'Halloran, T., 2005. Prediction accuracy for project wide evapotranspiration using crop coefficients and reference evapotranspiration. Journal of irrigation and drainage engineering. 131, 24-36. Recovery from: https://ascelibrary.org/doi/abs/10.1061/(ASCE)0733-9437(2005)131:1(24) (accessed 25 February 2023)

Baeza S., Rama G., Lezama F., 2019 Cartografía de los pastizales naturales en las regiones geomorfológicas de Uruguay predominantemente ganaderas. Ampliación y actualización. In: Altesor, A., López-Mársico, L., Paruelo, J.M. (Eds), Bases Ecológicas y tecnológicas para el manejo de pastizales II. Serie FPTA N° 69 INIA, Montevideo, pp. 27–47.

Baeza, S. and Paruelo, J. M., 2020. Land use/land cover change (2000–2014) in the Rio de la Plata grasslands: an analysis based on MODIS NDVI time series. Remote Sensing. 13:381. https://doi.org/10.3390/rs12030381

Baeza, S., Vélez-Martin, E., De Abelleyra, D., Banchero, S., Gallego, F., Schirmbeck, J., Verón, S., Vallejos, M., Weber, E., Oyarzabal, M., Barbieri, A., Petek, M., Guerra Lara, M., Sarrailhé, S. S., Balsi, G., Bagnato, C., Bruzzone, L., Ramos, S., Hasenack, H., 2022. Two decades of land cover mapping in the Río de la Plata grassland region: The MapBiomas Pampa initiative. Remote Sensing Applications: Society and Environment. 28:100834. https://doi.org/10.1016/j.rsase.2022.100834

Bajgain, R., Xiao, X., Wagle, P., Kimball, J. S., Brust, C., Basara, J. B., Woud, P., Starcks, P. J., Neel, J. P., 2020. Comparing evapotranspiration products of different temporal and spatial scales in native and managed prairie pastures. Remote Sensing. 13, 82. https://doi.org/10.3390/rs13010082

Bastiaanssen, W. G., Menenti, M., Feddes, R. A., Holtslag, A. A. M., 1998. A remote sensing surface energy balance algorithm for land (SEBAL). 1. Formulation. Journal of Hydrology. 212, 198-212. https://doi.org/10.1016/S0022-1694(98)00253-4

Bastiaanssen, W. G., Molden, D. J., Makin, I. W., 2000. Remote sensing for irrigated agriculture: examples from research and possible applications. Agricultural Water Management. 46, 137-155. https://doi.org/10.1016/S0378-3774(00)00080-9

Berger, A.G., Otero, A., Morales, X., Calistro, R., 2015. Actual Evapotranspiration Measurement Trough Eddy Covariance in Uruguay. Agrociencia Uruguay. 19:4. Recovery from: https://agrocienciauruguay.uy/index.php/agrociencia/article/view/240 (accessed 16 January 2023)

Bhattarai, N. and Wagle, P., 2021. Recent advances in remote sensing of evapotranspiration. Remote Sensing. 13, 4260. https://doi.org/10.3390/rs13214260

Bremer, D. J., Auen, L. M., Ham, J. M., Owensby, C. E., 2001. Evapotranspiration in a prairie ecosystem: effects of grazing by cattle. Agronomy Journal. 93, 338-348. https://doi.org/10.2134/agronj2001.932338x

Caselles, V., Artigao, M. M., Hurtado, E., Coll, C., Brasa, A., 1998. Mapping actual evapotranspiration by combining Landsat TM and NOAA-AVHRR images: application to the Barrax area, Albacete, Spain. Remote Sensing of Environment. 63, 1-10. https://doi.org/10.1016/S0034-4257(97)00108-9

Chang, Y., Qin, D., Ding, Y., Zhao, Q., Zhang, S., 2018. A modified MOD16 algorithm to estimate evapotranspiration over alpine meadow on the Tibetan Plateau, China. Journal of Hydrology. 561, 16-30. https://doi.org/10.1016/j.jhydrol.2018.03.054

Chao, L., Zhang, K., Wang, J., Feng, J., Zhang, M., 2021. A comprehensive evaluation of five evapotranspiration datasets based on ground and grace satellite observations: Implications for improvement of evapotranspiration retrieval algorithm. Remote Sensing. 13, 2414. https://doi.org/10.3390/rs13122414

Chapin, F. S., Matson, P. A., Vitousek, P. M., 2011. Principles of terrestrial ecosystem ecology. Springer, New York, NY.

Cleugh, H. A., Leuning, R., Mu, Q., Running, S. W., 2007. Regional evaporation estimates from flux tower and MODIS satellite data. Remote Sensing of Environment. 106, 285-304. https://doi.org/10.1016/j.rse.2006.07.007

Cihlar, J., Laurent, L. S., Dyer, J. A., 1991. Relation between the normalized difference vegetation index and ecological variables. Remote Sensing of Environment. 35, 279-298. https://doi.org/10.1016/0034-4257(91)90018-2

Cook, B. I., Smerdon, J. E., Seager, R., Coats, S., 2014. Global warming and 21st century drying. Climate Dynamics. 43, 2607-2627. https://doi.org/10.1007/s00382-014-2075-y

Cruz, G., Baethgen, W., Bartaburu, D., Bidegain, M., Giménez, A., Methol, M., Morales, H., Picasso, V., Podestá, G., Taddei, R., Terra, R., Tiscornia G. Vinocur, M., 2018. Thirty years of multilevel processes for adaptation of livestock production to droughts in Uruguay. Weather, Climate, and Society. 10, 59-74. https://doi.org/10.1175/WCAS-D-16-0133.1

Dai, A. (2013). Increasing drought under global warming in observations and models. Nature climate change. 3, 52-58. https://doi.org/10.1038/nclimate1633

Degano, M. F., Rivas, R. E., Carmona, F., Niclòs, R., Sánchez, J. M., 2021. Evaluation of the MOD16A2 evapotranspiration product in an agricultural area of Argentina, the Pampas region. The Egyptian Journal of Remote Sensing and Space Science. 24, 319-328. https://doi.org/10.1016/j.ejrs.2020.08.004

Decreto Nº. 366/018. Reglamentación de la Ley 16.858, referente al riego con destino agrario y regulación del aprovechamiento de las aguas del domino público. Recovery from: https://www.impo.com.uy/bases/decretos/366-2018#:~:text=En%20los%20casos%20de%20suministro,de%20Suelos%20y%20Aguas%20respectivo. (accessed 10 November 2022)

Di Bella, C. M., Rebella, C. M., Paruelo, J. M., 2000. Evapotranspiration estimates using NOAA AVHRR imagery in the Pampa region of Argentina. International Journal of Remote Sensing. 21, 791-797. https://doi.org/10.1080/014311600210579

Di Bella, C.M., Oricchio, P.A., Gusmerotti, L.A., Texeira, M., 2019. Updating of the algorithm estimation of real evapotranspiration (ETR) for the VIIRS-Suomi NPP sensor. Ecología Austral. 29, 428-432. 10.25260/EA.19.29.3.0.887

dos Santos, C. A., Mariano, D. A., Francisco das Chagas, A., Dantas, F. R. D. C., de Oliveira, G., Silva, M. T., da Silva, L. L., da Silva, B. B., Bezerra, B. G., Safa, B., Medeiros, S. S., Neale, C. M., 2020. Spatio-temporal patterns of energy exchange and evapotranspiration during an intense drought for drylands in Brazil. International Journal of Applied Earth Observation and Geoinformation. 85, 101982. https://doi.org/10.1016/j.jag.2019.101982

Faisol, A., Novita, E., 2020. An evaluation of MODIS global evapotranspiration product (MOD16A2) as terrestrial evapotranspiration in East Java-Indonesia. In IOP Conference Series: Earth and Environmental Science (Vol. 485, No. 1, p. 012002). IOP Publishing. Recovery from: https://iopscience.iop.org/article/10.1088/1755-1315/485/1/012002/meta (accessed 1 November 2022)

Falkenmark, M. and Rockström, J., 2006. The new blue and green water paradigm: Breaking new ground for water resources planning and management. Journal of water resources planning and management. 132, 129-132. Recovery from: https://www.eqb.state.mn.us/sites/default/files/documents/Falkenamark_20493345.pdf (accessed 10 November 2022)

Fisher, J. B., Malhi, Y., Bonal, D., Da Rocha, H. R., De Araujo, A. C., Gamo, M., Goulden, M. L., Hirano, T., Huete, A. R., Kondo, H., Kumagai, T., Loescher, H. W., Miller, S., Nobre, A. D., Nouvellon, Y., Oberbauer, S. F., Panuthai, S., Roupsard, O., Saleska, S., Tanaka, K., Tanaka, N., Tu, H. P., Von Randow, C., 2009. The land–atmosphere water flux in the tropics. Global Change Biology. 15, 2694-2714. https://doi.org/10.1111/j.1365-2486.2008.01813.x

Ford, C. R., Hubbard, R. M., Kloeppel, B. D., Vose, J. M., 2007. A comparison of sap flux-based evapotranspiration estimates with catchment-scale water balance. Agricultural and Forest Meteorology. 145, 176-185. https://doi.org/10.1016/j.agrformet.2007.04.010

Funk, C. Peterson, P. Landsfeld, M. Pedreros, D. Verdin, J. Shukla, S. Husak, G. Rowland, J. Harrison, Andrew, L., Michaelsen, J., 2015. The climate hazards infrared precipitation with stations-a new environmental record for monitoring extremes. Scientific Data. 2, 150066. https://doi.org/10.1038/sdata.2015.66

Giménez, L. and García Petillo, M., 2011. Summer crops evapotranspiration for two climatically contrasting regions of Uruguay. Agrociencia Uruguay. 15, 100-108. 19:4. Recovery from: http://www.fagro.edu.uy/agrociencia/revista/v15n2pdf/rcv15n2 (accessed 16 December 2022)

Gorelick, N., Hancher, M., Dixon, M., Ilyushchenko, S., Thau, D., Moore, R., 2017. Google Earth Engine: Planetary-scale geospatial analysis for everyone. Remote Sensing of Environment. 202:18-27. https://doi.org/10.1016/j.rse.2017.06.031

INIA-GRAS (2022). Unidad de Agro-clima y Sistemas de información del INIA. Recovery from: http://www.inia.uy/GRAS. (accessed 16 November 2022)

Guerschman, J. P., Van Dijk, A. I., Mattersdorf, G., Beringer, J., Hutley, L. B., Leuning, R., Pipunic, R. C., Sherman, B. S., 2009. Scaling of potential evapotranspiration with MODIS data reproduces flux observations and catchment water balance observations across Australia. Journal of Hydrology. 369, 107-119. https://doi.org/10.1016/j.jhydrol.2009.02.013

Gutiérrez, F., Gallego, F., Paruelo, J. M., Rodríguez, C., 2020. Damping and lag effects of precipitation variability across trophic levels in Uruguayan rangelands. Agricultural System. 185:102956. https://doi.org/10.1016/j.agsy.2020.102956

Hengl, T. and Gupta, S., 2019. Soil water content (volumetric%) for 33 kPa and 1500 kPa suctions predicted at 6 standard depths (0, 10, 30, 60, 100 and 200 cm) at 250 m resolution. Version v0, 1. Recovery from: https://zenodo.org/record/2784001 (accessed 16 October 2022)

INUMET, 2022. Instituto Uruguayo de Meteorología. Recovery from: https://www.inumet.gub.uy/clima/estadisticas-climatologicas/tablas-estadisticas (accessed 10 September 2022).

Jackson, R. D., Reginato, R. J., Idso, S., 1977. Wheat canopy temperature: a practical tool for evaluating water requirements. Water Resources Research. 13, 651-656. https://doi.org/10.1029/WR013i003p00651

Jasechko, S., Sharp, Z. D., Gibson, J. J., Birks, S. J., Yi, Y., Fawcett, P. J., 2013. Terrestrial water fluxes dominated by transpiration. Nature. 496, 347-350. https://doi.org/10.1038/nature11983

Kosugi, Y. and Katsuyama, M., 2007. Evapotranspiration over a Japanese cypress forest. II. Comparison of the eddy covariance and water budget methods. Journal of Hydrology. 334, 305-311. https://doi.org/10.1016/j.jhydrol.2006.05.025

Law Nº 16.858. Declaración de interés general el riego con desino agrario. Recovery from: https://www.impo.com.uy/bases/leyes/16858-1997 (accessed 01 November 2022)

Lessel, J., Sweeney, A., Ceccato, P., 2016. An agricultural drought severity index using quasi-climatological anomalies of remotely sensed data. International Journal of Remote Sensing. 37, 913-925. https://doi.org/10.1080/01431161.2016.1142689

Leuning, R., Zhang, Y. Q., Rajaud, A., Cleugh, H., Tu, K., 2008. A simple surface conductance model to estimate regional evaporation using MODIS leaf area index and the Penman-Monteith equation. Water Resources Research. 44(10). https://doi.org/10.1029/2007WR006562

Masek, J. G., Vermote, E. F., Saleous, N., Wolfe, R., Hall, F. G., Huemmrich, K. F., Gao, F., Kutler, J., Lim, T. K., 2012. LEDAPS Landsat calibration, reflectance, atmospheric correction preprocessing code. *ORNL DAAC*. Recovery from: https://doi.org/10.3334/ORNLDAAC/1146 (accessed 01 August 2022)

Milkovic, M., Paruelo, J. M., Nosetto, M. D., 2019. Hydrological impacts of afforestation in the semiarid Patagonia: A modelling approach. Ecohydrology. 12, e2113. https://doi.org/10.1002/eco.2113

Monteith, J. L., 1965. Evaporation and environment. In Fogg, G. E. (Ed.), The state and movement of water in living organisms. Cambridge, UK: Cambridge University Press. pp. 205–234.

Mu, Q., Heinsch, F. A., Zhao, M., Running, S. W., 2007. Development of a global evapotranspiration algorithm based on MODIS and global meteorology data. Remote sensing of Environment. 111, 519-536. https://doi.org/10.1016/j.rse.2007.04.015

Mu, Q., Zhao, M., Running, S. W., 2011. Improvements to a MODIS global terrestrial evapotranspiration algorithm. Remote Sensing of Environment. 115, 1781-1800. https://doi.org/10.1016/j.rse.2011.02.019

Munka, C., Pezzani, F., Caffera, M., 2013. Effects of silvilcultural management on leaf area and evapotranspiration in Pinus taeda in northeastern Uruguay. Agrociencia Uruguay. 17, 55-63. https://doi.org/10.31285/agro.25.429

Navas, R., Tiscornia, G., Berger, A. G., Otero, A., 2021. Assessing MODIS16A2 actual evapotranspiration across three spatial resolutions in Uruguay. Agrociencia Uruguay [Internet]. https://doi.org/10.31285/AGRO.25.429

Nosetto, M. D., Jobbágy, E. G., Paruelo, J. M., 2005. Land-use change and water losses: the case of grassland afforestation across a soil textural gradient in central Argentina. Global Change Biology. 11, 1101-1117. https://doi.org/10.1111/j.1365-2486.2005.00975.x

Nosetto, M. D., Jobbágy, E. G., Brizuela, A. B., Jackson, R. B., 2012. The hydrologic consequences of land cover change in central Argentina. Agriculture, Ecosystems & Environment. 154, 2-11. https://doi.org/10.1016/j.agee.2011.01.008

Otero, A., Berger, A. G., Morales, X., Calistro, R., 2015. Eddy Covariance Estimates of Evapotranspiration in Irrigated and Rainfed Soybean in Uruguay. Agrociencia Uruguay. 19:8 Recovery from: https://agrocienciauruguay.uy/index.php/agrociencia/article/view/244 (accessed 15 February 2022)

Oyarzabal, M., Andrade, B., Pillar, V. D., Paruelo, J. M., 2020. Temperate Subhumid Grasslands of Southern South America. In: Goldstein, M. I., Della Sala, D. A. (Eds.), Encyclopaedia of the World's Biomes, Elsevier, pp. 577-593. https://doi.org/10.1016/B978-0-12-409548-9.12132-3

Panario, D., Gutiérrez, O., Sánchez Bettucci, L., Peel, E., Oyhantçabal, P., Rabassa, J., 2014. Ancient landscapes of Uruguay. In Gondwana landscapes in southern South America (pp. 161-199). Springer, Dordrecht. https://doi.org/10.1007/978-94-007-7702-6_8

Paruelo, J. M., Jobbágy, E. G., Oesterheld, M., Golluscio, R. A., Aguiar, M. R., 2007. The grasslands and steppes of Patagonia and the Rio de la Plata plains. In: Veblen, T. T., Young, K. R., Orme A. R. (Eds.) The physical geography of South America, pp. 232-248.

Paruelo, J. M., 2008. La caracterización funcional de ecosistemas mediante sensores remotos. Ecosistemas, 17(3). Recovery from: https://www.revistaecosistemas.net/index.php/ecosistemas/article/view/83 (accessed 01 November 2022)

Paruelo, J. M., Texeira, M., Staiano, L., Mastrángelo, M., Amdan, L., Gallego, F., 2016. An integrative index of Ecosystem Services provision based on remotely sensed data. Ecological Indicators. 71, 145-154. https://doi.org/10.1016/j.ecolind.2016.06.054

Qin, Z., Karnieli, A., Berliner, P., 2001. A mono-window algorithm for retrieving land surface temperature from Landsat TM data and its application to the Israel-Egypt border region. International Journal of Remote Sensing. 22, 3719-3746. https://doi.org/10.1080/01431160010006971

R Core Team (2021). R: a language and environment for statistical computing. R Foundation for Statistical Computing, Vienna, Austria. http://www.Rproject.org

Rienecker, M. M., Suarez, M. J., Gelaro, R., Todling, R., Bacmeister, J., Liu, E., Bosilovich, M. G., Schubert, S. D., Takacs, L., Kim, G., Bloom, S., Chen, J., Collins, D., Conaty, A., da Silva, A., Gu, W., Joiner, J., Koster, R. D., Lucchesi, R., Molod, A., Owens, T., Pawson, S., Pegion, P., Redder, C. R., Reichle, R., Robertson, F. R., Ruddick, A. G., Sienkiewicz, M., Woollen, J., 2011. MERRA: NASA's modern-era retrospective analysis for research and applications. Journal of Climate. 24, 3624-3648. https://doi.org/10.1175/JCLI-D-11-00015.1

Rockström, J., Gordon, L., Folke, C., Falkenmark, M., Engwall, M., 1999. Linkages among water vapor flows, food production, and terrestrial ecosystem services. Conservation Ecology, 3(2). https://www.jstor.org/stable/26271715

Roy, D. P., Borak, J. S., Devadiga, S., Wolfe, R. E., Zheng, M., Descloitres, J., 2002. The MODIS land product quality assessment approach. Remote Sensing of Environment. 83, 62-76. https://doi.org/10.1016/S0034-4257(02)00087-1

Running, S. W., Mu, Q., Zhao, M., Moreno, A., 2017. MODIS global terrestrial evapotranspiration (ET) product (NASA MOD16A2/A3) NASA earth observing system MODIS land algorithm. *NASA: Washington, DC, USA*. Recovery from: https://landweb.modaps.eosdis.nasa.gov/QA_WWW/forPage/user_guide/MOD16UsersGuide2016V1.52017May23.pdf (accessed 05 October 2022)

Salemi, L. F., Groppo, J. D., Trevisan, R., de Moraes, J. M., de Paula Lima, W., Martinelli, L. A., 2012. Riparian vegetation and water yield: a synthesis. Journal of Hydrology. 454, 195-202. https://doi.org/10.1016/j.jhydrol.2012.05.061

Sanchez, J. M. and Caselles, V., 2004. Determining actual evapotranspiration in a boreal forest. Recent Research Developments in Geophysics. Vol. *6*, pp. 59-80.

Schlesinger, W. H. and Jasechko, S., 2014. Transpiration in the global water cycle. Agricultural and Forest Meteorology. 189, 115-117. https://doi.org/10.1016/j.agrformet.2014.01.011

Silveira, L., Gamazo, P., Alonso, J., Martínez, L., 2016. Effects of afforestation on groundwater recharge and water budgets in the western region of Uruguay. Hydrological Processes. 30, 3596-3608. https://doi.org/10.1002/hyp.10952

Soriano, A., León, R. J. C., Sala, E. O., Lavado, R. S., Dereguibus, V. A., Cahuepé, M. A., Scaglia, O. A., Velázquez, C. A. Lemcoff, J. H., 1991. Rio de la Plata Grasslands. In: Coupland (ed.) Ecosystems of the world 8A. Natural grasslands. Introduction and Western Hemisphere. 1st edn. New York. Elsevier. pp 367-407.

Trenberth, K. E., Fasullo, J. T., Kiehl, J., 2009. Earth's global energy budget. Bulletin of the American Meteorological Society. 90, 311-324. https://doi.org/10.1175/2008BAMS2634.1

Velpuri, N. M., Senay, G. B., Singh, R. K., Bohms, S., Verdin, J. P., 2013. A comprehensive evaluation of two MODIS evapotranspiration products over the conterminous United States: Using point and gridded FLUXNET and water balance ET. Remote Sensing of Environment. 139, 35-49. https://doi.org/10.1016/j.rse.2013.07.013

Viets, F. G., 1962. Fertilizers and the efficient use of water. Advances in Agronomy, 14, 223-264. https://doi.org/10.1071/AR9660255

Vörösmarty, C. J., Green, P., Salisbury, J., Lammers, R. B., 2000a. Global water resources: vulnerability from climate change and population growth. Science. 289, 284-288. https://doi.org/10.1126/science.289.5477.284

Vörösmarty, C. J. and Sahagian, D., 2000b. Anthropogenic disturbance of the terrestrial water cycle. Bioscience. 50, 753-765. https://doi.org/10.1641/0006-3568(2000)050[0753:ADOTTW]2.0.CO;2

Vörösmarty, C. J., Hoekstra, A. Y., Bunn, S. E., Conway, D., Gupta, J., 2015. Fresh water goes global. Science. 349, 478-479. https://doi.org/10.1126/science.aac6009

Wilson, K. B., Hanson, P. J., Mulholland, P. J., Baldocchi, D. D., Wullschleger, S. D., 2001. A comparison of methods for determining forest evapotranspiration and its components: sap-flow, soil water budget, eddy covariance and catchment water balance. Agricultural and forest Meteorology. 106, 153-168. https://doi.org/10.1016/S0168-1923(00)00199-4

Xu, T., Guo, Z., Xia, Y., Ferreira, V. G., Liu, S., Wang, K., Yai, Y., Zhang, X., Zhao, C., 2019. Evaluation of twelve evapotranspiration products from machine learning, remote sensing and land surface models over conterminous United States. Journal of Hydrology. 578, 124105. https://doi.org/10.1016/j.jhydrol.2019.124105

Yang, Y., Long, D., Shang, S., 2013. Remote estimation of terrestrial evapotranspiration without using meteorological data. Geophysical Research Letters. 40, 3026-3030. https://doi.org/10.1002/grl.50450

Yu, Q., Zhang, Y., Liu, Y., Shi, P., 2004. Simulation of the stomatal conductance of winter wheat in response to light, temperature, and CO2 changes. Annals of Botany. 93, 435-441. https://doi.org/10.1093/aob/mch023

Zhang, Y., Kong, D., Gan, R., Chiew, F. H., McVicar, T. R., Zhang, Q., Yang, Y., 2019. Coupled estimation of 500 m and 8-day resolution global evapotranspiration and gross primary production in 2002–2017. Remote Sensing of Environment. 222, 165-182. https://doi.org/10.1016/j.rse.2018.12.031